Special Contributions, Geophysical Institute, Kyoto University, No. 4, 1964, 153-192

ON THE SEQUENCE OF EARTHQUAKES

By

Hikaru WATANABE

(Received October 31, 1964)

Abstract

In and near Kinki District, many microearthquakes of seismic magnitude from less than zero up to about 1 or 2 are occurring almost stationarily. But they are classified into several earthquake sequences according to the space distribution of their foci and the time series of their occurrence.

With the help of the elastic rebound theory, the characteristics of these sequences of microearthquakes were investigated in relation to that of severe earthquakes of M 5 or more. As the result, it could be concluded that the seismic activity at a certain region was clearly characterized by the main shock and its beforeshock and aftershock sequences and also that the sequence structure of earthquake swarms might be adequately explained by the rheological models with the help of the experimental results on rock deformation and an application of the rate process theory to the rheological materials in the earth's interior.

Contents

Introduction
Chapter I Seismometric observations
1. Seismometers
2. Seismograms of microearthquakes
3. Space distribution of foci of the microearthquakes and time series of their occurrence
4. Sequences of severe earthquakes
5. Frequency distribution of the maximum amplitudes
6. Elastic rebound theory
7. Characteristics of sequences
Chapter II Laboratory experiments on rock deformation and their relation to earthquake phenomena
1. Types of rock creep
2. Mechanism of rock creep
3. Observation of elastic shocks caused by fractures of rocks
4. An application of the rate process theory to the fracturing effect on the rock creep
5. Sequence structure of the before and after shocks
Chapter III Summary
Appendix

Introduction

At Abuyama Seismological Observatory the routine seismological observation

is being made with various seismometers. Among these seismometers, SH-II and OA type seismometers having high magnifications at short periods have frequently registered swarms of microearthquakes with hypocentral distances less than several tens of a kilometer as well as the swarms of the severer earthquakes occurring in and near Kinki District, Central Honshu, Japan.

One of the main purposes of this paper is to consider the questions why many earthquakes occur in succession within a certain confined region and what would be the characteristics of the mechanism of their occurrence.

In the following chapters, several examples of the earthquake swarms will be treated from two standpoints, that is, an analysis of the seismological data and a discussion on the relations between the seismic phenomena and the experimental results on the deformation of rocks and other materials subjected to high pressures.

Chapter I. Seismometric observation

1. Seismometers

In and near Kinki District, many earthquakes of M (seismic magnitude) from less than zero up to about 5 or 6 are occurring almost 'stationarily', and one of the main purposes of the present study is to investigate the occurrence of these microearthquakes in relation to that of destructive earthquakes of M 5 or more. Most of them are observed by various seismometers of different types at Abuyama Seismological Observatory, which belongs to the Faculty of Science, Kyoto University.

Since the predominant period of seismic waves caused by microearthquakes is shorter than 1 sec., highly sensitive seismometers of short period are required in order to register very small earthquakes having hypocentral distances less than several tens of a kilometer. One of the highly sensitive seismometers used for routine operation at the observatory is OA type horizontal seismometer, which adopts an electrodynamic transducer and a C-R amplifier to obtain an extremely high magnification at short periods less than 1 sec. SH-II type seismometer having a magnification of 2×10^4 at a period of 0.6 sec. is also suitable for the observation of microearthquakes.

The amplitude of short period ground unrests observed at the observatory is ordinarily about 0.1 μ or less at a frequency of 10 cps. And hence we can get a better S/N ratio at the observatory than at ordinary city areas.

On the other hand, a different type seismometer is required for the observation of large earthquakes having hypocentral distances less than several hundred kilometers. For this purpose we used the records of S-1000 seismometer, which has a pendulum of 1 ton in weight and a smoked paper recording system. These seismometers are firmly fastened to the bed rock, which is geologically composed of Palaeozoic system.

The constants of the seismometers and their magnification curves are shown in Table 1 and Fig. 1 respectively.

Table 1. Constants of seismographs

Seismograph	V max.	T_1	T_2	h_1	h_2	σ	ρ
SH-II (Z)	22,000	1.06	1.20	1.00	1.32	0.31	
(E)	19,000	0.86	1.08	1.00	1.00	0.11	
(N)	20,000	0.83	1.08	1.00	1.00	0.15	
OA (N)	10,000	0.76	0.7	1.0	0.5		0.2
S-1000 (Z)	870	1.1		0.4			0.5
(E)	850	1.2		0.4			0.5
(N)	850	1.2		0.4			0.5

T_1: Period of pendulum (sec.)
T_2: Period of galvanometer (sec.)
h_1: Damping constant of pendulum
h_2: Damping constant of galvanometer
σ : Coupling factor
ρ : Solid friction (m/m)

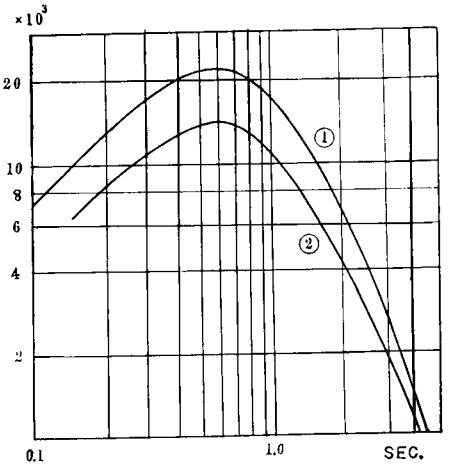

Fig. 1. Magnificatoin curves of the seismographs.
①: SH-II type seismograph
②: OA type seismograph

2. Seismograms of microearthquakes

When the records of microearthquakes are extremely masked by ground unrests, we must detect these traces by comparing many seismograms recorded at different points several hundred meters apart, because the records of an earthquake registered at those positions should be quite similar.

But in this study the discrimination between earthquake motions and disturbances

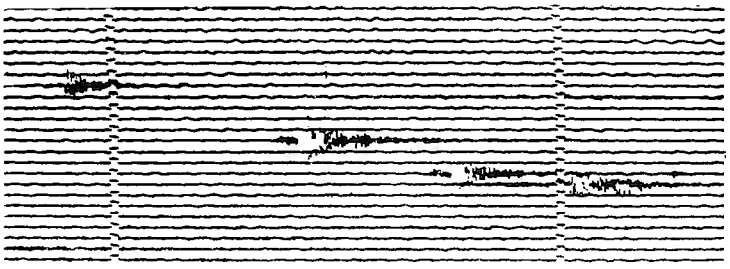

Fig. 2. An example of seismograms obtained by SH-II type seismograph. ($00^h46^m \sim 04^h53^m$, 8th June 1959. Time mark: every 1 minute)

was made merely by comparing the wave forms of one vertical and two horizontal components, because we could ordinarily get a good S/N ratio at the observatory except in the case of stormy weather.

Fig. 2 is an example of seismograms of the microearthquakes having hypocentral distances of several tens of a kilometer obtained by SH-II type seismometer. In examining these seismograms, the following points can be clearly noticed:

1) Many shocks seem to occur successively within a small confined volume of the earth's crust, because their wave forms are quite similar to each other and the P-S intervals of these seismograms surely fall in 2.7 ± 0.05 sec.

2) The amount of energy sent out from the origin of the microearthquakes in the form of seismic waves can be determined by integrating the kinetic energy throughout the traces of earthquakes. However, we may roughly estimate the kinetic energy of the earthquakes by use of the maximum velocity amplitude of shear waves and the duration of vibration, because the amplitude of shear waves is extremely large in comparison with the other waves.

3) As is well known, the predominant period of seismic waves, when recorded by a certain seismometer, becomes longer with the increase of both magnitude and hypocentral distance. However, waves with periods of $0.2 \sim 0.4$ sec. are always superposed on the main part of the seismograms as may be seen from the traces in Fig. 2.

This phenomenon has been studied by many authors considering refraction, reflection and scattering of the seismic waves in the earth's interior. According to their explanations (Kanai et al., [1954]; Omote et al., [1956]), it is probably the results of superposition of waves which arise from an effect of the layered system of the observation station.

3. Space distribution of foci of microearthquakes and time series of their occurrence

During the observation period, about two hundreds of microearthquakes with

P-S intervals less than 5 sec. were recorded by OA type seismometer. And their foci were roughly determined by use of P-S intervals and also initial directions of the seismic P waves in order to analize the space distribution of origins of the microearthquakes.

When the initial motions were small and masked by disturbances of ground unrests, the wave forms of later phases were also adopted for the determination of their foci under the assumption that the wave forms which travelled through a nearly same path may be quite similar to each other.

The P-S interval is approximately proportional to the hypocentral distance, however, the frequency distribution of the P-S intervals does not always represent the space distribution of foci themselves.

But the direction of the approach of initial P wave in horizontal plane can be derived from the vectorial resultant of the initial motions in two horizontal components. And by use of the orientation thus estimated, and also by use of the P-S intervals, the foci of the microearthquakes were roughly determined under an assumption of homogeneous medium.

A plot of the epicenters of the microearthquakes having P-S intervals less than

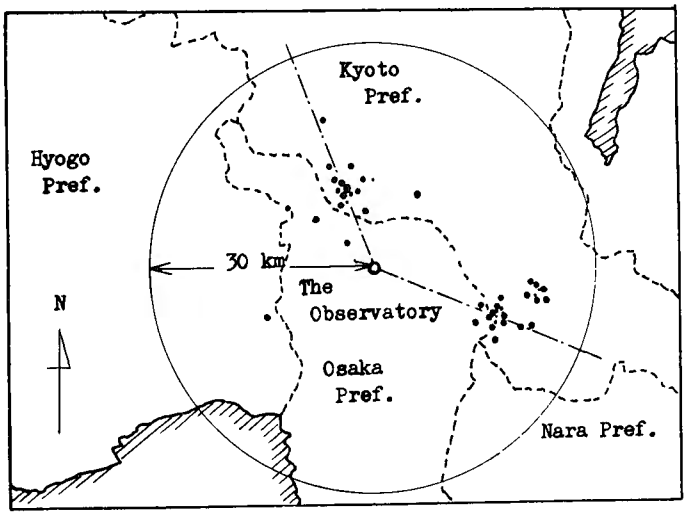

Fig. 3. Distribution of epicenters of microearthquakes with P-S intervals less than 5 sec., whose initial P waves were clearly recorded by SH-II type seismometers during 1959.

5 sec. is shown in Fig. 3. It may be seen from this figure that the distribution of the epicenters is divided into two decided areas whose respective orientations are: E 20°S

for the earthquakes with P-S intervals of 2.5～3.5 sec. and N 25°W for the earthquakes with P-S intervals of 1.5～2.0 sec.

Thus the microearthquakes occurred in 1959 are classified into the two groups according to the space distribution of their foci and let us call them A group (P-S intervals: 2.5～3.5 sec.) and B group (P-S intervals: 1.5～2.0 sce.) respectively.

An example of plots of P-S intervals against occurrence times of the earthquakes

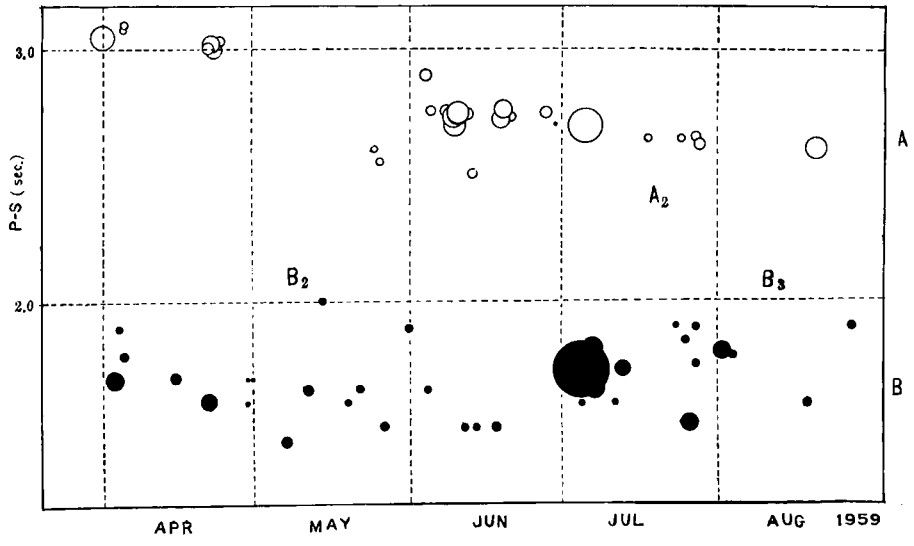

Fig. 4. A plot of occurrence times against P-S intervals of microearthquakes. The diameters of the circles are in proportion to the maximum amplitudes of earthquakes.

is illustrated in Fig. 4, in which the earthquakes belonging to A and B groups are denoted respectively by open and solid circles whose diameters are, in turn, proportional to the maximum trace amplitudes of shocks.

From these figures, it is clearly concluded that the microearthquakes can be classified into several groups according not only to the space distribution of their foci but also to the distribution of their occurrence times. On the basis of these facts, the earthquakes belonging to A and B groups can be again divided into subgroups (A_1, A_2, ⋯ and B_1, B_2, ⋯) as tabulated in Table 2.

Since the area of each circle in Fig. 4 may be approximately proportional to the energy released from the origin, it is easy to detect from the appearance of the circles that there are two typical patterns in energy radiation. More concretely speaking, the earthquakes belonging to, e.g. B_3 group occur after the main shock and the rate of energy radiation is decreasing monotonically with time. This pattern of energy radiation is quite similar to that of aftershocks accompanying a severe earthquake.

Table 2. List of sequences occurring near Abuyama in 1959

Sequence	Duration	Number of earthquakes	Ultimate strain*
A_1	3 Jan. 14 Mar.	26	84
A_2	4 June - 3 Nov.	36	210
A_3	3 Nov. - 30 Jan. (1960)	21	72
B_1	5 Feb. 26 Feb.	9	17
B_2	2 Apr. 5 July	31	90
B_3	5 July 30 Aug.	18	39
B_3	8 Oct. 22 Dec.	25	98

* Measured on a conventional scale (cf. Figs. 9 and 10)

On the other hand, the shocks belonging to, e.g., A_2 and B_2 groups occur at a nearly constant rate of energy radiation. Therefore they are not aftershocks of a particular earthquake.

Furthermore it is very interesting to note that the two types of earthquake groups stated above occur in contact with a major shock. For example, a major earthquake of M about 3 occurred on 3rd July 1959. Before and after its occurrence many minor shocks were observed as shown in Fig. 4 and the foci of these shocks (belonging to B_2 and B_3 groups) are surely confined to a very small volume of the earth's crust. It may be consequently inferred that the major shock and the two types of earthquake groups may compose a series of seismic activity at the region in the earth's crust. These facts are equally true of the earthquakes of A_2 and A_3 groups as will be described in later sections. Accordingly, let us call them (the two types of earthquake groups occurring before and after the principal shock) the 'beforeshock sequence' and 'aftershock sequence' respectively.

4. Sequence of severe earthquakes

Severe earthquakes are frequently accompanied by many aftershocks which occur with almost similar mechanism to that of the main shock. And many seismic phenomena regarding the occurrence of aftershocks have been successfully studied by many investigators from various standpoints, though some problems still remain unsolved.

Among these problems, it is very interesting and important to see whether severe earthquakes are accompanied by not only aftershocks but also beforeshocks as was seen in the case of microearthquake, and also whether the sequences of severe earthquakes have the characteristics similar to that of the microearthquakes.

The following is a study on these questions by using a sequence of severe earthquakes which occurred in the area about 100 km apart from the observatory.

In 1961, about 200 earthquakes occurred in succession from April to June at the

region near Himeji, Central Honshu, Japan. The largest earthquake was observed on May 7, and its magnitude and focal depth were estimated to be about 6.3 and 10 km respectively by Japan Meteorological Agency.

Selecting 6 major shocks out of the swarm of the earthquakes, their occurrence times, magnitudes, focal depths and the location of their epicenters determined by J.M.A. are illustrated in Fig. 5. A large number of somewhat slighter earthquakes

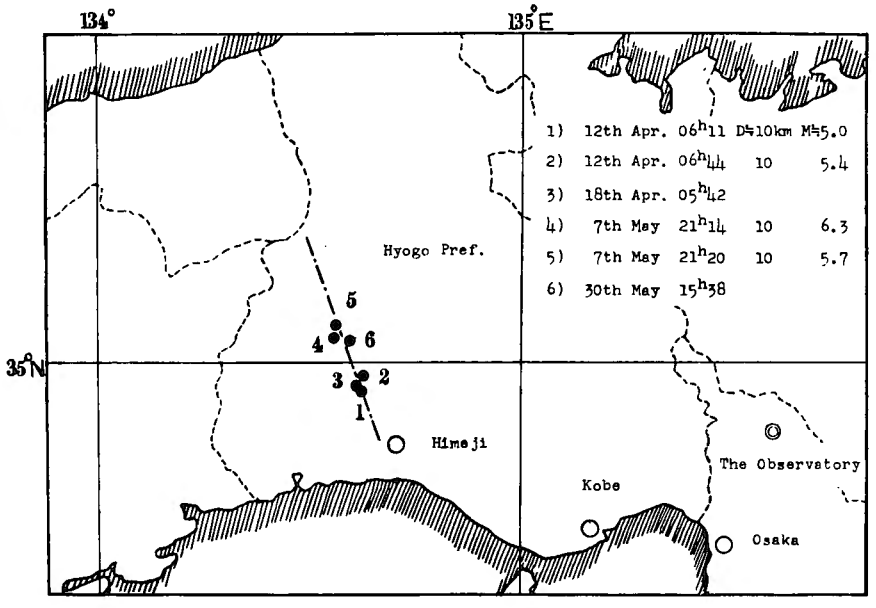

Fig. 5. Location of epicenters of the principal earthquakes.

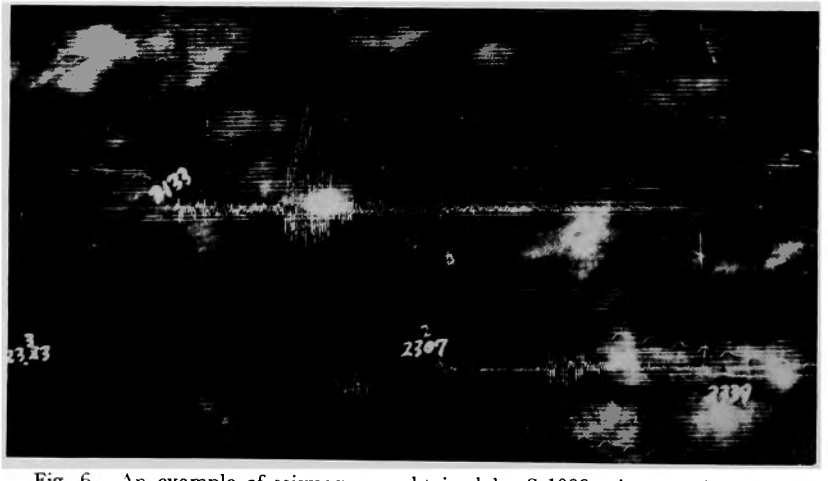

Fig. 6. An example of seismograms obtained by S-1000 seismograph (EW). (21^h30^m~23^h40^m, 7th May 1961. Time mark: every 1 minute)

were also observed at the observatory and an example of seismograms obtained by S-1000 seismometer is shown in Fig. 6. As may be seen from these seismograms, the epicenters of minor shocks seem to be distributed close to that of the major shocks.

In fact, the determinations of their epicenters by use of both P-S intervals and the directions of initial P motions show clearly that they are distributed within the long and slender area studded with the epicenters of the major shocks, as shown in Fig. 5.

The distributions of the initial motions of 4 principal shocks, including the main shock which occurred on May 7, are given in Fig. 7. And the so called quadrant type

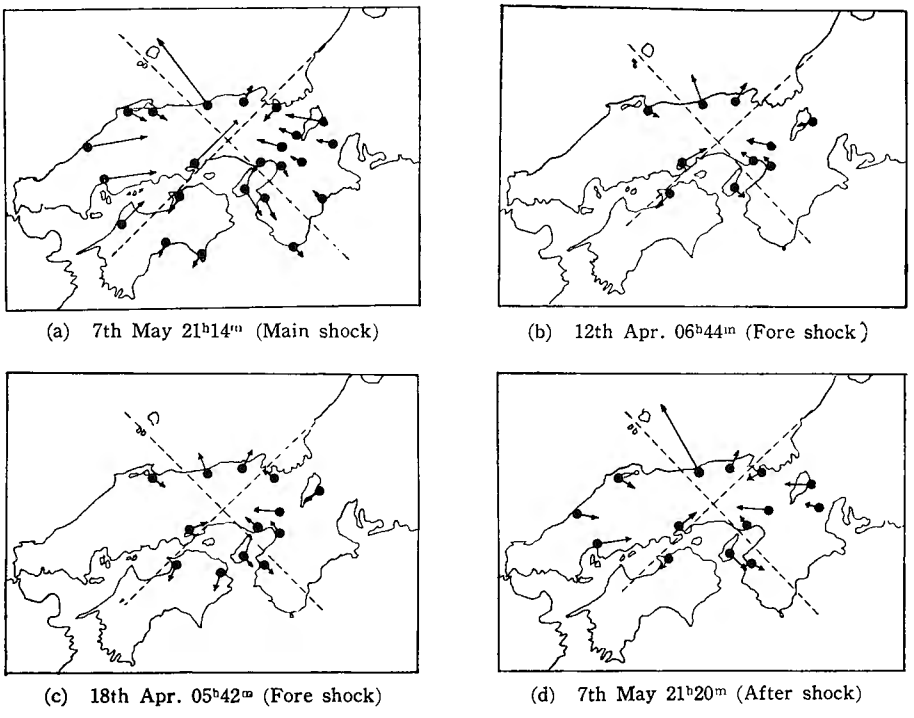

(a) 7th May 21^h14^m (Main shock) (b) 12th Apr. 06^h44^m (Fore shock)

(c) 18th Apr. 05^h42^m (Fore shock) (d) 7th May 21^h20^m (After shock)

Fig. 7. Push-pull distributions of initial motions of P waves.

pattern in which the earth's surface is divided into four quadrants by two straight lines crossing at the epicenter is clearly ascertained and, furthermore, the minor shocks accompanying the main shock seem to have a similar pattern to that of the main shock. In fact, the quadrant type patterns of initial P waves are frequently ascertained for earthquakes of shallow foci. For explanation of this pattern of initial P waves, there are two prevailing hypotheses on earthquake mechanism and they will be discussed in some detail in Appendix, considering the strike slip fault theory with the help of experimental results on fracturing mechanism of rocks. On the basis of

these facts, it is inferred that the stress distribution causing the main shock may remain for the duration of earthquake occurrence.

Many of the minor shocks which occurred prior to the main shock surely form a group of earthquakes in accordance with the time distribution of their occurrence and it may be eventually regarded as a beforeshock sequence, because the time rate of their occurrence or the rate of energy radiation is nearly constant. On the other hand, the minor shocks which occurred after the main shock may plausibly belong to the category of the aftershock sequence, because they accompany the main shock and are occurring at a decreasing rate of energy radiation. Consequently, a series of seismic activity at the region near Himeji is composed of the two types of seismic sequences, i.e., the beforeshock sequence and the aftershock sequence.

More detailed information on this aspect is to be studied in later sections with reference to the sequences of microearthquakes.

5. Frequency distribution of the maximum amplitudes

The number of earthquakes occurring in a certain area may be always dependent on their magnitudes and the problems on the frequency distribution of magnitude have been studied by many investigators from the various standpoints. In studying these problems, it is desirable to determine the magnitude of every earthquake. However, it is technically difficult to carry out the accurate determination of magnitude of individual earthquake. Therefore, it is convenient to adopt the empirical relation of the frequency distribution of trace amplitudes under an assumption that the decay of seismic waves depends only on the properties of the medium and not on the magnitude of the earthquakes.

According to the study by Ishimoto and Iida [1939], the relation concerning the frequency distribution of trace amplitude a is expressed by the equation

$$N(a)da = ka^{-m}da\,, \qquad (1)$$

where k is an appropriate constant conerning the period of observation as well as the seismic activity of a certain closed region and it is considered that the value of m may characterize a certain seismic region being studied. However, the equation (1) is only an empirical equation and is not derived theoretically, and the frequency distribution of magnitudes can be expressed by some other equations derived, e.g. by Komura [1954, 1955]. Nevertheless, the empirical equation has been of great use in studying the statistical seismology.

Fig. 8 is an illustration of frequency distribution of trace amplitudes of the microearthquakes above metioned, where A, B and T are computed for the earthquakes belonging to A and B groups and for total earthquakes respectively. From

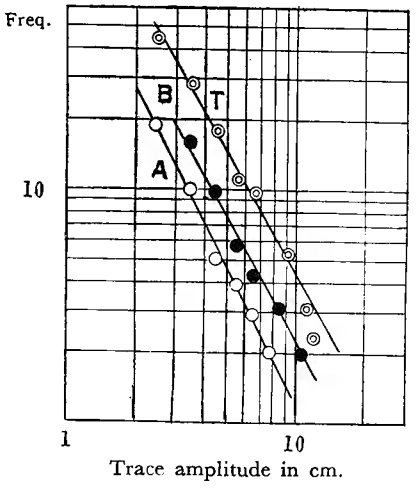

Fig. 8. Frequency distribution of trace amplitudes. The graphs A, B and T are computed for the earthquakes belonging to A and B groups and for the total earthquakes respectively.

the graphs, the values of m are calculated as 1.92 and 1.80 for A and B groups presectively.

It is generally ascertained that the value of m ranges about 1.7 to 1.9 for earthquakes occurring in a certain seismic region in Japan except for the volcanic earthquakes. Therefore, the values of 1.92 and 1.80 for A and B groups are compatible with those results up to date and the slight difference between them may not always represent the difference of the seismic activity between both regions. Accordingly, the value of 1.76 for total earthquakes is also statistically significant.

Thus, the results given from this figure show that the equation (1) is valid for the relation in the occurrence of microearthquakes as well as of large earthquakes, and it is very interesting to investigate whether the relation expressed by the formula (1) holds good within a wider range of magnitude from less than zero up to 5 or 6.

Asada and his coworkers [1954, 1959] have already made the observation of microearthquakes by use of ultra-sensitive seismometers at Tsukuba and Matsushiro, Central Honshu, Japan. As the results of the observation, they have shown that the empirical formula holds good for the microearthquakes of M less than zero up to about 5 and also that the value of m is about 1.9 even for the earthquakes having M less than zero.

On the other hand, a series of laboratory experiments on fracturing of several materials made by Mogi [1962a, 1962b] have shown that the parameter m varies widely with brittleness of the materials and elastic shocks which are probably caused by the local fracture of the materials may be closely related to earthquake phenomena.

In recent year, Miyamura [1962] suggested that the parameter surely represented the characteristics of a certain seismic region, with the help of the geotectonic survey over the world.

In order to clarify these problems, more of field evidence must be collected. And as a matter of fact, the consecutive observation of microearthquakes may provide the data for inferring the occurrence of destructive earthquakes.

6. Elastic rebound theory

According to Reid's suggestion [1911], it is assumed that tectonic earthquakes are generally produced by elastic release of strained rocks in the earth's interior and the elastic energy is emitted in the form of seismic waves.

When an average elastic strain ε is assumed to be distributed uniformly in an effective volume V of the strained rock, the strain energy stored up in the rock is given by

$$E = \tfrac{1}{2}\mu\varepsilon^2 V, \qquad (2)$$

where μ is the appropriate elastic constant of the rock just before the outbreak of earthquake.

Tsuboi [1956] has assumed that the energy of an earthquake is mainly dependent on the effective volume of the strained rock and also that $\frac{1}{2}\mu\varepsilon^2$ (the maximum energy to be stored up within an unit volume of rock) is $3\times10^3\sim2\times10^4$ C.G.S. throughout the earth's crust. On the other hand, a controversial view was suggested by Benioff [1951a, 1951b], in which he considered that the energy of an earthquake is determined by the crustal strain ε rather than the effective volume V.

In the present study, let us consider μV in equation (2) constant for the duration of a sequence of earthquakes according to Benioff's suggestion, because earthquakes belonging to a certain sequence are occurring wholly within a small confined volume of the earth's crust and the earthquake generating force acting at the focal region is sure to remain unchanged for the duration of earthquake occurrence, as shown in the previous sections.

If the strain energy stored up within a confined volume of the strained rock is released entirely during a sequence of earthquakes and if a fraction p of the stored energy is converted into seismic waves and it remains unchanged throughout the sequence, the energy of an individual earthquake is given by

$$e_i = \tfrac{1}{2}p\mu\varepsilon_i^2 V = C^2\varepsilon_i^2, \qquad (3)$$

where $C^2=\frac{1}{2}p\mu V$ is constant.

Thus, the total seismic energy for a given sequence is calculated from the next equation,

$$J = pE = c^2\Sigma\varepsilon_i^2 . \qquad (4)$$

On the other hand, the kinetic energy of spherical seismic wave with a radius r is expressed by

$$e_i' = 2\pi r^2 v \cdot \tfrac{1}{2}\sigma\tau_i a_i^2 , \qquad (5)$$

where v : velocity of the spherical waves,
σ : density of the medium,
τ_i: duration of oscillation, and
a_i: velocity amplitude.

When the spherical waves are assumed to decay according to the formula e^{-hr}/r, the equation (5) must be corrected for the decay effect of e^{-hr}, in order to obtain the value of the energy radiated from the hypocenter, because the effect of $1/r$ is already involved in the equation (5). The value of h is 0.02 km^{-1} according to Kawasumi [1952] for the waves with a period of 0.3 sec. Thus, the value of e^{-hr} for the micro-earthquakes belonging to A group is evaluated as 0.67, where r is about 20 km. The maximum deviation from the mean hypocentral distance is estimated to be about 8 km as the result of the observations and errors due to a change in the hypocentral distance in calculating the energy of earthquakes are merely less than 5 percents. As already shown, the foci of earthquakes belonging to a certain sequence are distributed within a small confined volume of the earth's crust. And their hypocentral distances are large in comparison with the size of the seismic region and, therefore, they can be assumed to be nearly constant for a given sequence.

Furthermore, the velocity of the seismic waves v and the density of the medium σ are also considered to be nearly constant for a given sequence. Therefore, the equation (5) is rewritten as follows:

$$e_i' = k^2\tau_i a_i^2 , \qquad (6)$$

where $k^2 = 2\pi r^2 v \cdot \frac{1}{2}\sigma e^{2hr}$ is constant for a given sequence. Then, equating (3) with (6) and extracting the released strain, we have

$$\varepsilon_i = C\sqrt{\tau_i}\, a_i , \qquad (7)$$

where $C = k/c$. Hereupon, it is considered that C is constant for a given sequence, whereas it may vary according to the conditions in the mechanism of the earthquake occurrence at the focal region of individual sequences, in other words, may vary according to stress difference for overcoming the friction of the fault wall, stress rate of the tectonic force, ultimate strength of the medium and so on.

In the previous sections, the characteristics of the occurrence pattern of earthquakes were studied with the help of the space distribution of their foci and the

distribution of their occurrence times. More detailed informations on this aspect are to be considered in the next section by means of the procedure stated above.

7. Characteristics of sequences

In Figs. 9 and 10, the cumulative sums of elastic strain releases for every sequence are plotted against their occurrence times and the two types of sequences of Himeji

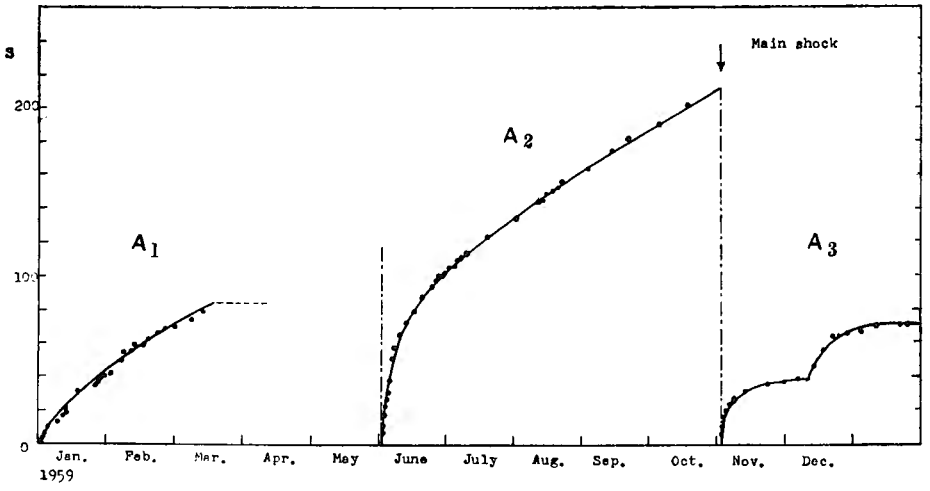

Fig. 9. Cumulative sums of elastic strain releases for the sequences belonging to A group.

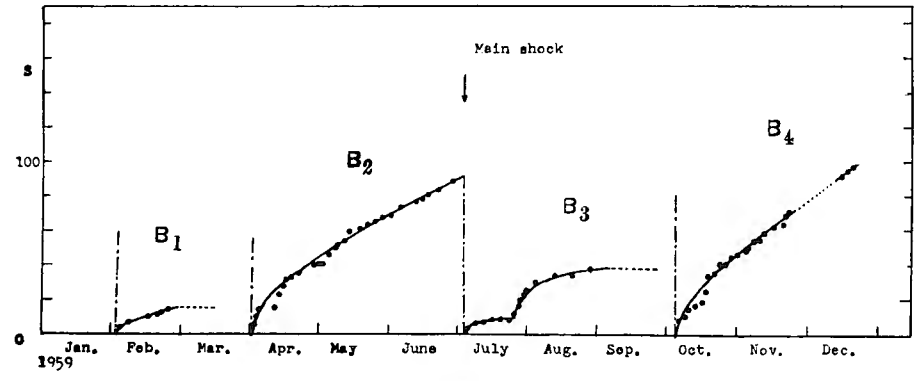

Fig. 10. Cumulative sums of elastic strain releases for the sequences belonging to B group.

earthquakes are also illustrated by the graphs of C_1 and C_2 in Fig. 11.

The constant C in equation (7) may differ with different sequences as stated in the preceding section. But it may be possible to reject it in plotting the cumulative sum, because we are able to see the characteristics of sequences merely from the

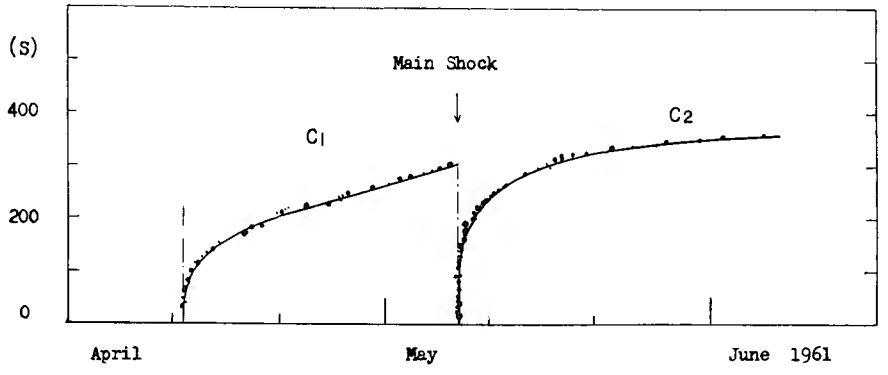

Fig. 11. Cumulative sums of elastic strain releases for Himeji sequences.

patterns of these graphs. Accordingly, $\Sigma\sqrt{\tau_i}\,a_i$ was calculated directly from the seismograms and plotted, instead of $\Sigma\varepsilon_i$, in arithmetical coordinates.

In these figures, the arrows denote the occurrences of the main shocks, whose elastic strain releases are not summed up here, and the dotted lines represent the temporary pause of seismic activity. In examining these graphs, the following points can be apparently noticed:

1) The main shocks are sure to occur between the two different types of sequences and a series of seismic activity certainly continues for the duration of the two different types of sequences. More concretely speaking, the beforeshock sequence, e.g. B_2 sequence began after some pause of seismic activity and lasted until the outbreak of the main shock. Then the aftershock sequence, e.g. B_3 sequence started to occur and continued for a while and at last the seismic activity at the region came to end.

2) As may be seen from the graphs of A_3 and B_3, the aftershock sequences of microearthquakes are composed of the two different patterns of strain release as was already studied by Benioff [1951a, 1951b] in the case of aftershock sequences of severe earthquakes. On the contrary, the graph of C_2 is apparently represented by only a monotonous curve, which will be regarded as a special case of aftershock sequences, as will be described later.

3) The graphs of beforeshock sequences, e.g. A_2, B_2 and C_1 are remarkable for their simplicity, that is, the linear relation shown in these graphs may characterize the beforeshock sequence so that we can easily distinguish the beforeshock sequence from the aftershock sequence.

4) The other graphs of A_1, B_1 and B_4 are quite similar to that of the beforeshock sequence, though they are not accompanied by both the main shock and the other sequence. These isolated sequences have been sometimes observed in routine operation at the observatory. This phenomena may be presumably explained as follows: the main fracture throughout the focal region does not take place if the

amount of accumulated stress does not exceed the strength of the composing materials, however, if the materials have somewhat weaker parts which are distributed irregularly throughout the materials, a part of the accumulated stress may be released little by little producing minor fractures at the weaker parts of the materials. This is only a hypothesis, however, and more detailed information on this problem would be desirable in order to ascertain the mechanism of fracture occurrence.

5) It is noteworthy that, regardless of the amounts of the released energies summed up for the duration of sequences, the graphs of the beforeshock sequence and of the early part of the aftershock sequence of microearthquakes are quite similar in shape to those of the respective sequences of Himeji earthquakes. Moreover, it must be emphasized that, both in cases of the microearthquakes and the severe earthquakes, the occurrence patterns of the series of seismic activities (which are composed of the main shock and the beforeshock and aftershock sequences as mentioned above) are closely resemble each other in their appearances.

Now, these graphs are rewritten and plotted anew on semi-logarithmic papers as shown in Figs. 12, 13 and 14, for the purpose of studying the characteristics of the occurrence patterns of the series of seismic activities in more detail. In these figures, the abscissae are occurrence times of each earthquake measured in days from the first shock of the particular sequence. Therefore, the aftershock sequence begins with the outbreak of the main shock, which is denoted by the arrow.

As may be seen from these graphs, the cumulative sum of released strain for the aftershock sequence is, in general, well expressed by

$$S = A+B\log t+C\exp(-D\sqrt{T}), \qquad (8)$$

where A, B, C and D are appropriate constants and $T=t-t_0$ (t_0 is the interval of the early part of the aftershock sequence).

The graph C_2 is, however, made up of the straight line alone, which, in turn, coincides with the early part of the aftershock sequence of the microearthquakes and it is presumably inferred that the constant C in equation (8) may be so small that the secondary part of the sequence cannot be distinguished from the graph of C_2.

On the other hand, the following equation,

$$S = a+b\log t+ct, \qquad (9)$$

always holds good for the beforeshock sequences, where a, b and c are appropriate constants. The third term in equation (9) is prominant at the later part of the beforeshock sequence and may characterize this type of sequence distinctly.

As already stated, it is highly important that the simple equations such that equations (8) and (9) may well represent the characteristics of the beforeshock and aftershock sequences without reference to the amount of the released energy summed

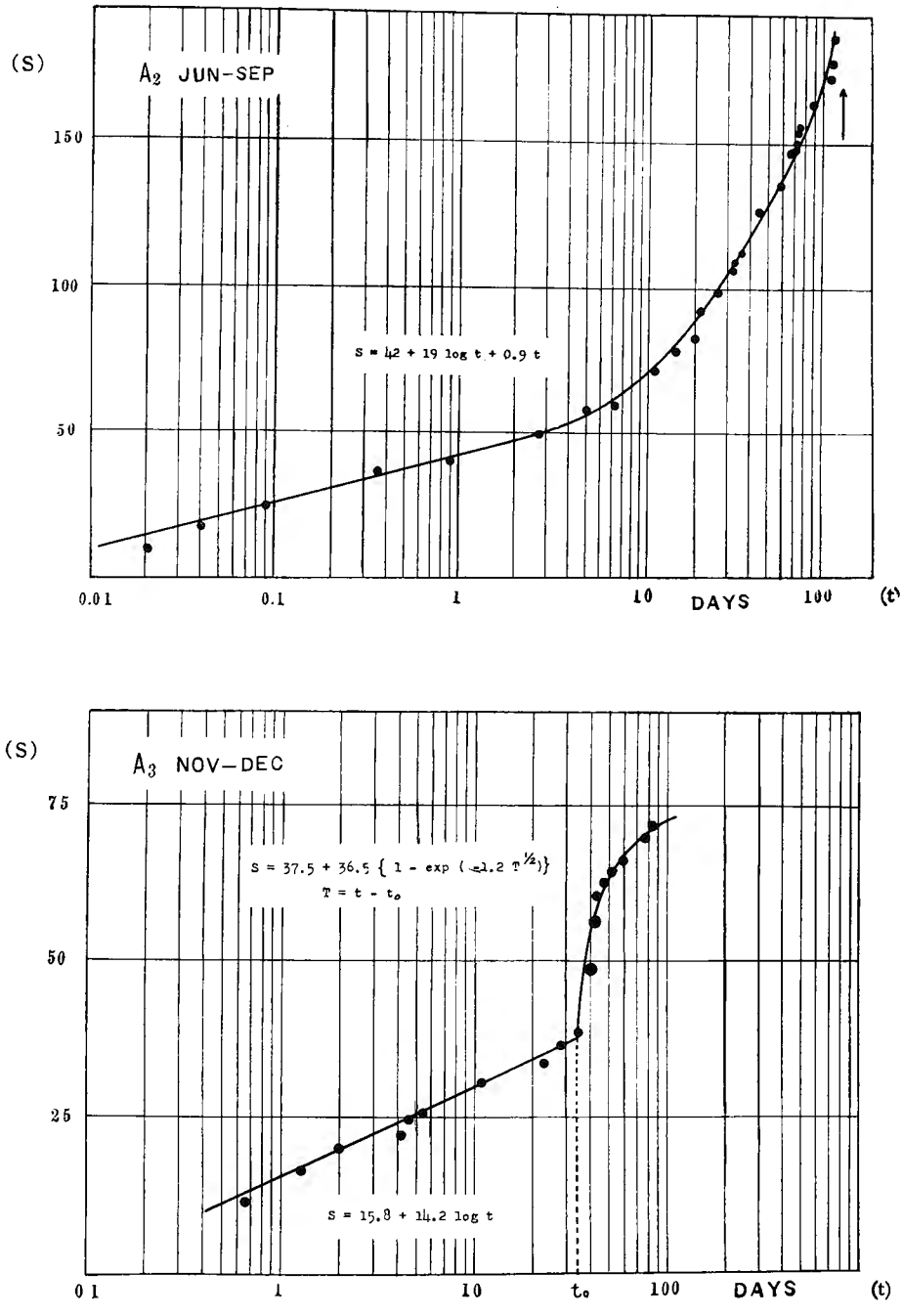

Fig. 12. A_2 and A_3 sequences plotted on semi-logarithmic papers.

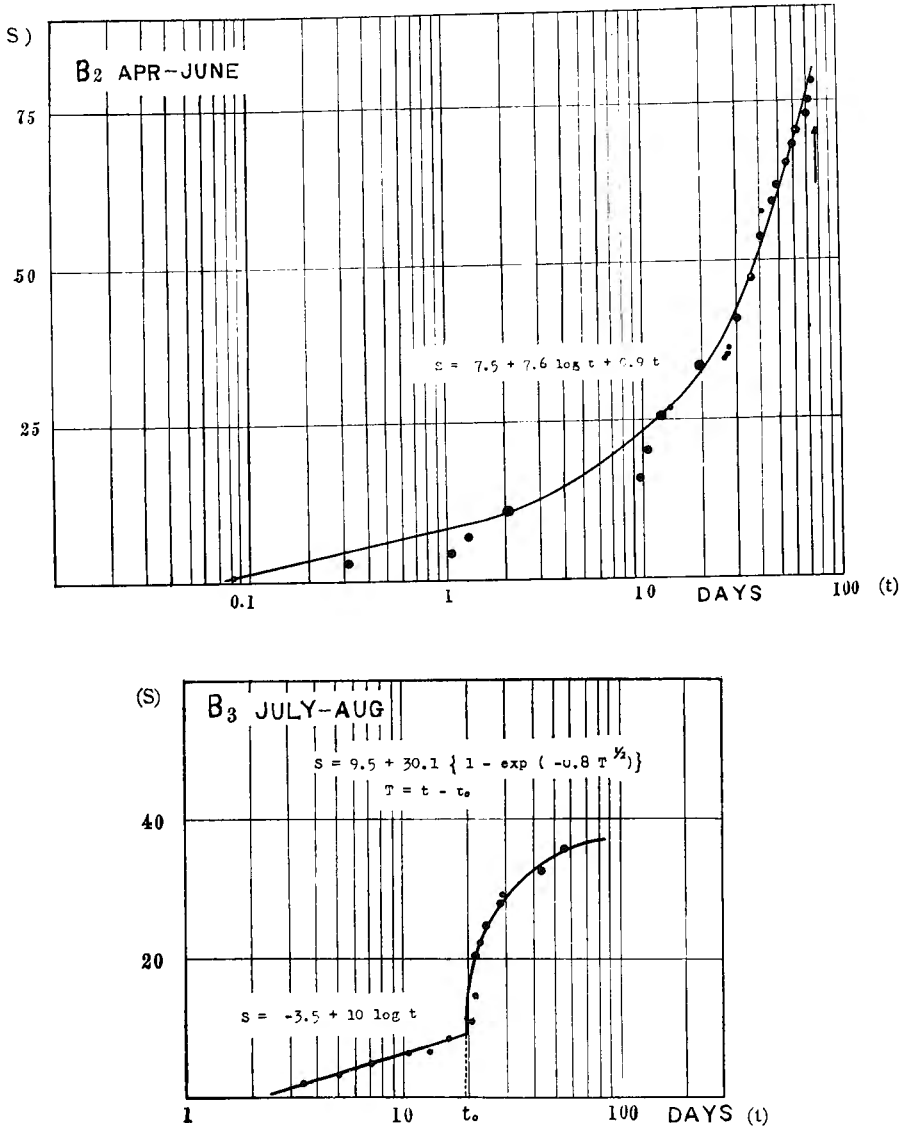

Fig. 13. B_2 and B_3 sequences plotted on semi-logarithmic papers.

up for the duration of a sequence. This fact may give a suggestion that the routine observation of successive occurrence of earthquakes with highly sensitive seismometers installed widely over the seismic active region may provide valuable data on the occurrence of destructive earthquake with the help of the procedure stated above. Hence, we are espccially interested in the questions by what cause the series of earth-

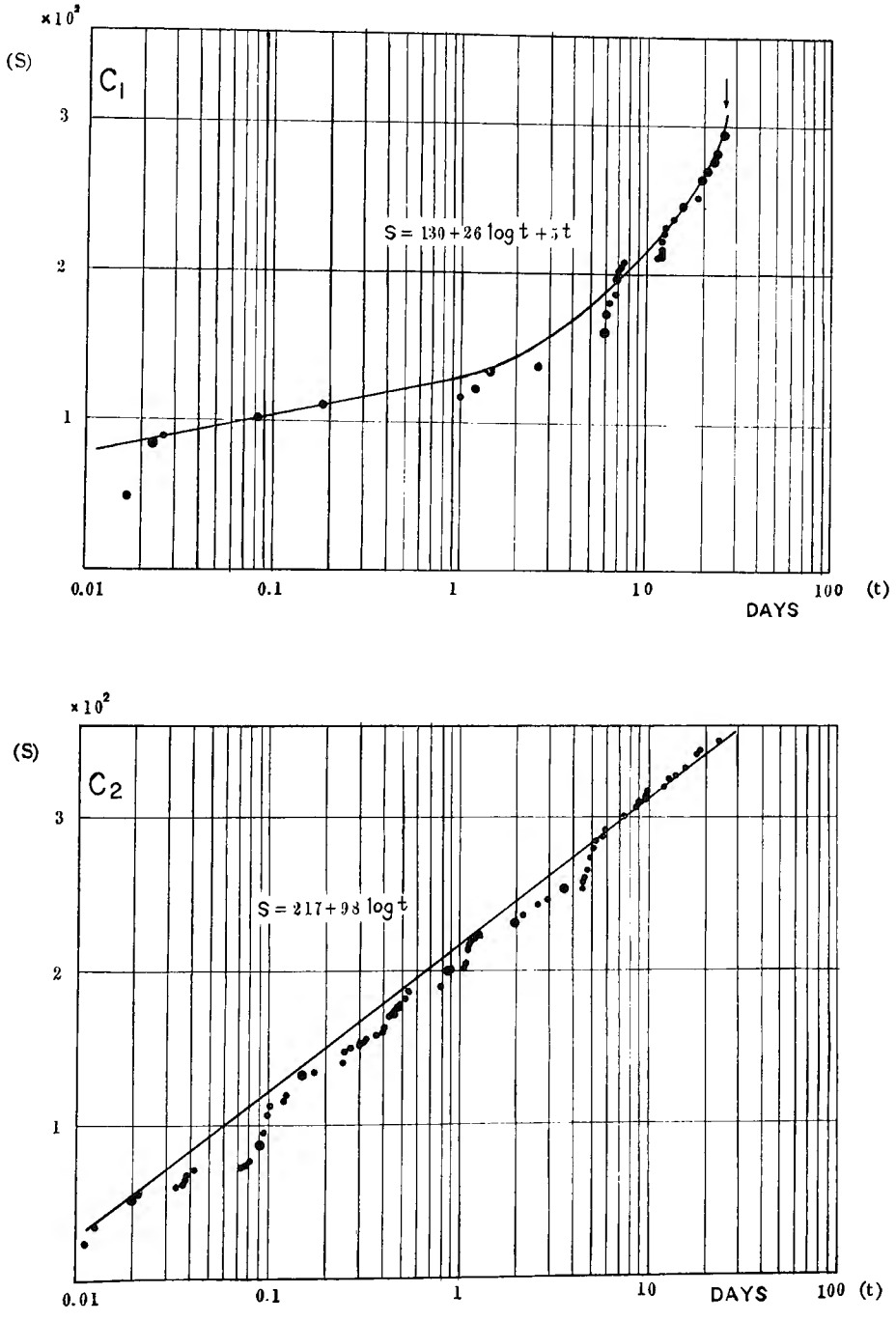

Fig. 14. C_1 and C_2 sequences plotted on semi-logarithmic papers.

quake sequences are produced and why the empirical relations (8) and (9) hold always good, despite the fact that the amount of energy released for the druation of the series of seismic activities differs greatly with different sequences.

In the following chapter, some discussions on these problems will be studied in relation to laboratory experiments on creep and fracturing of rock specimens subjected to high pressures.

Chapter II. Laboratory experiments on rock deformation and their relation to earthquake phenomena

1. Types of rock creep

Various experiments by many investigators have shown that a rock specimen may sustain a certain static stress for a while, but the same stress may break down the specimen, when stressed for longer duration. Among these investigators, Griggs [1940], Lomnitz [1956] and others have studied the creep of various rocks and minerals under compression. And a thorough analysis of the creep data has been made to try to relate them to the mechanism of deformation of the rocks, considering the empirical relations among strain, time and stress conditions. In practice, when a sample is loaded axially under a continuous stress at the time $t=0$, the resulting creep increases with time following the typical curve as shown in Fig. 15.

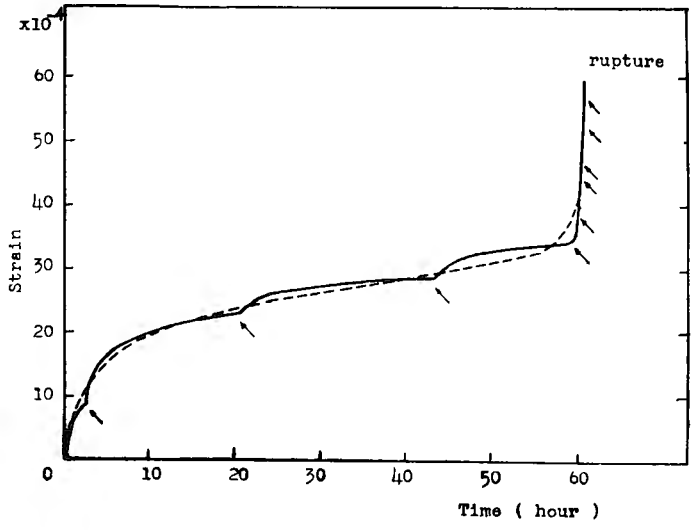

Fig. 15. An example of creep curves observed in lateral direction. Arrows denote appreciable fractures. (after Matsushima, [1960])
Solid line : Observed value
Dotted line: Normal creep curve

As well known, these strain-time curves can be divided into three portions designating the types of creep: 1) the initial range of "transient creep" with rapidly increasing strain which is followed by decelerating strain, 2) the range of "steady-state creep" where the strain is linear with time and 3) the range of "accelerating creep" in which the strain is accelerated to the rupture. However, only the first stage appears in the creep measurements carried on for relatively short perids of time. In order to observe the linear secondary stage and the final stage, the sample must be stressed highly enough or it must be loaded for a longer duration at high temperatures. These problems on the stages of creep were discussed and summarized, e.g. by Handin [1957].

According to his experimental results, the empirical strain-time relation both for the transient creep and the steady-state creep is given by

$$S = p + q \log t + rt \,, \tag{10}$$

where p, q and r are constant both for a given specimen and for a given confining pressure. This relation holds fairly well for the creep curves of most rocks and minerals tested previously by Griggs and Lomnitz and also for the curve shown in Fig. 15.

2. Mechanism of rock creep

At present, several possibilities to explain the mechanism of rock deformation have been discussed, considering fracturing, gliding, recrystallization and intragranular slip. Among them, the fracturing defined as a breaking of cohesion with slippage through and around grains in crystalline rocks seems to be of great importance in studying the mechanism of rock deformation.

Orowan [1949] has also suggested that, in the process of stress application, all rocks may be deformed principally by fracturing and he discussed on the occurrence of deep earthquakes in some detail on the basis of this conception.

Evidence supporting fracturing as an important mechanism of creep was found by Bridgman [1949] in measuring the abnormal volume change with increasing stress. His discovery is that under uniaxial stress the length and volume of specimen decrease linearly with increasing stress according to the ordinary experience up to a limiting value of compressional stress, but at a load only slightly beyond this limit of linear elasticity the volume increases sharply, whereas the length is decreasing, and in the initial stages of release of load the volume decreases instead of increasing as it would be expected in the elastic range. This abnormal increase of volume, according to his explanation, can be ascribed to an opening of the interstices in the structure as a premonition of the fracture and this recovery proceeds further during release of load so that only a small fraction of the abnormal volume increase at the maximum load is

permanently retained on total release of load.

Another evidence for fracturing in creep of Solenhofen limestone under increasing load was given by Robertson [1960]. He observed the significant decrease in the densities of the specimens deformed under confining pressures up to 4,000 bars and under stress differences from 3,000 to 8,000 bars at room temperature. These decreases in density occurred probably because of the increase of the bulk volume, which may be due to expansion across the fracture surface. According to the result of his experiment (Table 3), the elastic strain which recovers instanteneously with

Table 3. Changes in length and in density after removal of hydrostatic pressure, in percentages of original length and original density (2.601 g/cc) measured by Robertson [1960] on Solenhofen limestone

Specimen No.	Average P (bars)	Residual strain after removing P (%)	Strain recovered by removing P (%)	Residual change of density (%)
S-83	350	−13.2	1.8	−12.3
S-82	750	−12.0	4.0	− 8.9
S-86	1,000	−16.3	3.3	−11.2
S-89	2,000	−27.4	3.9	−10.7
S-90	3,000	−15.1	3.6	− 3.7
S-88	4,000	−17.5	4.2	− 4.3

release of confining pressure would not exceed 1 percent and the large recovery of longitudinal strain (column 4 of Table 3) is mostly from nonelastic strain corresponding to the transient creep, which is, in turn, due to fracturing of rocks. Fracturing, therefore, is an important mechanism of the transient creep at low pressure.

On the other hand, a portion of rock deformation retains permanently after removing the pressure (column 3 of Table 3), when the specimens are stressed highly enough or stressed for longer duration at high temperatures.

In accordance with many experiments (see, e.g., Matsushima's report [1960]), the permanent deformation of rocks is sure to correspond to the steady state creep in which the strain increases in linear with time and this process may actually be explained as fracturing with subsequent healing. More concretely speaking, rocks loaded under a nearly constant pressure for longer duration may deform by fracturing but, thereafter, the fracturing will heal with the pressure acting on the fracture surface so that it is invisible to the naked eye. Thus, cohesion of rocks is retained by partial healing of fractures, especially in the case of very small fractures under high confining pressures. Moreover, experiments show that the deformation recovers according only to the second term of the empirical relation (10). Accordingly, it may be concluded that, in the forward process of rock creep, the second and third terms of the empirical relation well represent the transient creep (recoverable creep on total

release of load) and the steady state creep (permanent deformation) respectively.

Now, let us return to the creep curve shown in Fig. 15. The arrows denote the appreciable fractures which are visible in thin sections under the microscope and the significant increase of deformation is observed concurrently with occurrence of fractures. If the deformation of rocks is caused by fracturing as stated above, the increments of creep will certainly coincide with the occurrences of many fractures and the greater the number of fractures, the nearer the observed value approaches the normal creep curve, which is, in turn, well expressed by the empirical strain-time relation.

3. Observation of elastic shocks accompanied by fractures of rocks

In a recent experiment by the present writer [1963], relations between the mechanisms of the normal creep and the occurrences of many fractures were studied in some detail.

Solid cylinders of granite, marble, dunite and sandstone were axially compressed into the plastic range or beyond their strength, under atmospheric pressure at room temperature and the elastic shocks caused by fractures of the rock specimens were observed by an acoustic method. Murata's $BaTiO_3$ ceramic vibrator was set on the specimens as a transducer of the elastic shocks and the signals were amplified by an amplifier with a transmission band of 30～10,000 cps and were recorded by an electromagnetic oscillograph having a natural period of 0.01 sec. The strain in the process of stress application was also measured by a Shinko-type electric resistance strain meter.

By using traces of the elastic shocks, relative energy was calculated as a square of maximum amplitude, that is, $E=k\cdot a^2$, where a is the maximum trace amplitude and k is a constant.

Under the assumption that an average elastic strain ε may be distributed uniformly within the volume V of the strained rock specimen, the strain energy was estimated as $E'=\mu\varepsilon^2 V/2$, where μ is an elastic constant. If a fraction p of the elastic strain energy is converted into wave energy when an elastic shock occurs inside the rock specimen, E is given by $E=pE'$ and the elastic strain is expressed by

$$\varepsilon = K\sqrt{E} = K_1 a\,, \tag{11}$$

where $K^2=2/(p\mu V)$ and $K_1^2=2k/(p\mu V)$.

With the help of equation (11), the summation of ε of successive shocks $\Sigma\varepsilon$ or $\Sigma\sqrt{E}$ was calculated and plotted against time in Fig. 16 for the granite specimen, which was compared with the strain curve of the granite specimen. As may be seen

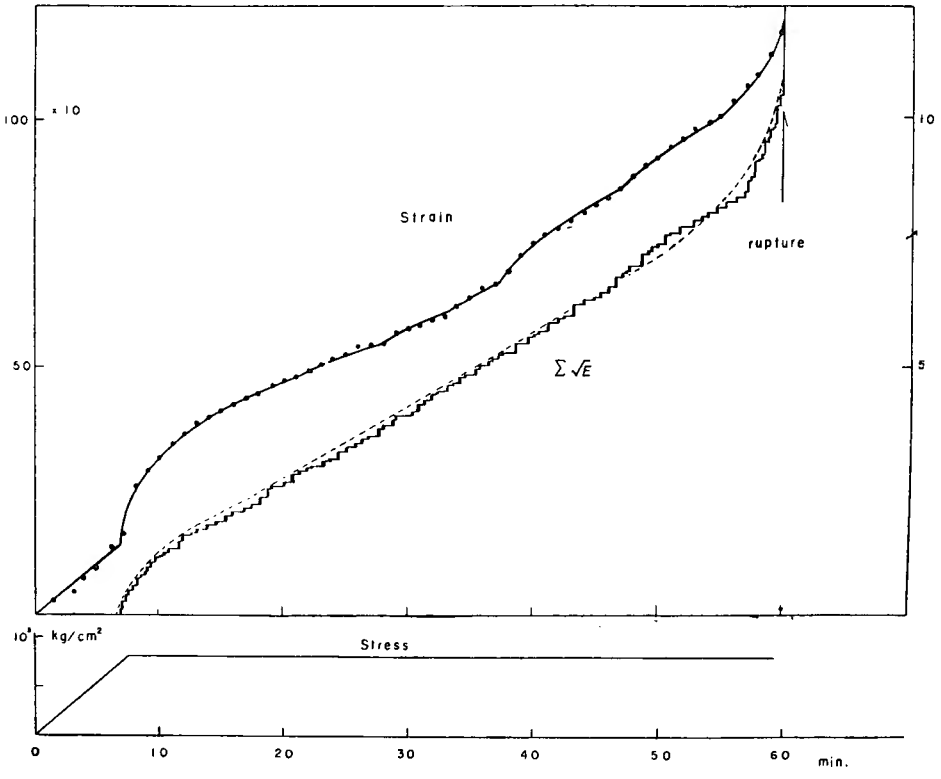

Fig. 16. Strain curve of granite measured in lateral direction and cumulative sum of the square root of elastic energy of successive shocks in arbitrary unit.

Table 4. Characteristics of the rocks

	Granite	Marble	Dunite	Sandstone
Elastic ultimate strain	15×10^{-4}	7.0×10^{-4}	11×10^{-4}	0.9×10^{-4}
Non-elastic ultimate strain	105×10^{-4}	19×10^{-4}	17×10^{-4}	1.0×10^{-4}
Number of elastic shocks	105	85	69	15
$\Sigma\sqrt{E}$*	10.5	3.3	2.6	0.4
Heterogeneity of materials**	highly heterogeneous	heterogeneous	heterogeneous	nearly homogeneous

* Measured on a conventional scale
** Examined under the microscope

from this graph, in so far as the strain has a linear relation with the applied stress of comparatively short duration, no elastic shock occurs. But at the beginning of the non-linear strain, a number of elastic shocks begin to take place abruptly and thereafter they occur at a constant rate until they again begin to increase and at last the main rupture takes place throughout the specimen. And it is highly important to note that the pattern of $\Sigma\sqrt{E}$ changes in parallel with the strain curve throughout the stages

of the rock creep. Furthermore, the characteristics of the rocks summarized in Table 4 show apparently that the non-elastic ultimate strain of respective rocks varies remarkably and systematically with the number of shocks or with the value of $\Sigma\sqrt{E}$ and also that they indicate approximately the degree of heterogeneity of the respective rocks.

As described in the preceding sections, the non-elastic ultimate strain is composed of two kinds of rock deformations such that the recoverable and irrecoverable deformations on total release of load, which, in turn, coincide with the transient and steady state stages in creep curve respectively. Then, the forward process of the creep curve shown in Fig. 16 is also well expressed by the empirical relation throughout the non-elastic stages of creep curve, however, in the rebound process of the rock creep, the third term of the empirical relation will vanish, because the permanent deformation caused by partial healing of fractures is sure to retain for ever.

On the basis of these facts, it is clarified that the elastic shocks are caused by the local brittle fractures and the mechanism of the non-elastic striain or the creep of rocks is closely related with the occurrence of the local fractures inside the rock specimens. More concretely speaking, at the moment when the stress is applied, an instantaneous elastic strain is produced in the specimen, which is wholly recovered concurrently with release of the stress. But the strain energy having been stored up in the specimen under the continuous application of constant stress is partially converted into elastic energy concurrently with the occurrence of local fractures.

Thus, the effect of fracturing on the mechanism of the rock creep may be well explained by the facts that the pattern of $\Sigma\sqrt{E}$ is quite similar to the normal creep curve as seen in Fig. 16 and also that the numbers of elastic shocks indicate approximately the degree of brittleness of the respective rocks.

4. An application of the rate process theory to the fracturing effect on the rock creep

Surveys of theoretical attempts to general and rational analyses of deformation mechanism of rocks have been made by many investigators, but no complete theoretical basis for explaining the effect of fractures on the creep of rocks have been established as yet. However, there is evidence that some problems on non-elastic deformation of rocks are adequately explained by use of the rheological theory.

The rheological behavior of rocks is determined by an equation between stress and deformation and also by their derivatives with respect to time, and the rheological equation and its parameters characterize the materials being studied.

In practice, elasticity and viscosity are fundamental properties of rheology and for these fundamental properties the following models have been suggested:

a) A helical spring representing the Hooke body with

$$P = El_1 , \tag{12}$$

where E is Young's modulus of the spring, and P and l_1 are the resultants of all external forces acting on the spring and the contraction of the spring respectively.

b) A dash pot representing the Newtonian liquid with

$$P = \eta \frac{dl_2}{dt} , \tag{13}$$

where η is the viscosity coefficient of the dash pot and l_2 is its displacement.

These elements may be coupled in parallel or in series for explaining the bodies with complex rheological properties. When coupled in parallel, the pressures taken by each one of the elements are additive while the rate of contraction of them is the same. When coupled in series, the rates of contraction of them are additive, while each one of them takes the total pressure.

In order to represent the delayed elasticity in regard to the elastic before and after effects of rock deformation, the Kelvin body has been proposed. The model for the Kelvin body is composed of a pure spring and a dash pot being combined in parallel as shown in Fig. 17.

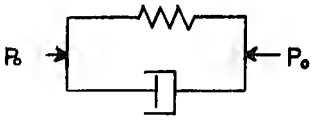

Fig. 17. Model for Kelvin body.

Adding a constant pressure P_0 on the body, we get

$$P_0 = El_1 + \eta \frac{dl_2}{dt} , \tag{14}$$

by use of equations (12) and (13). The parameter of viscosity in equation (14) is generally assumed to be constant with consequent simplification of integration, but it is actually variable as examined by Eyring and his coworkers [1941]. According to Eyring's theory of rate process, the rate of strain of the viscous element in Fig. 17 may be written as

$$\frac{dl_2}{dt} = K \sinh (\alpha p) , \tag{15}$$

where p is partial pressure acting on the dash pot. In this equation K is a function of molecular parameter including the activation energy for the flow process, and $\alpha = a\lambda / 2kT$, where a is a cross sectional area of the flow unit, λ is the distance between equilibrium positions of the flow unit, k is the Boltzman constant and T is

the absolute temperature. A more detailed discussion of this definition of K and α is given in Eyring's book [1941]. Thus, K and α in equation (15) can be assumed to be constant for a given body.

Since the pressure p on the dash pot is $p=P_0-El_1$ and $l_1=l_2$, equation (15) is rewritten as

$$\frac{dl_2}{dt} = K\sinh\alpha(P_0-El_2)\,. \tag{16}$$

When p and $P_0\alpha$ are large, we can write as a resonable close approximation,

$$\frac{dl_2}{dt} = \frac{K}{2}\exp\left[\alpha(P_0-El_2)\right],$$

which becomes,

$$\frac{dl_2}{\exp\left[\alpha(P_0-El_2)\right]} = \frac{K}{2}\,dt\,, \tag{17}$$

in separating the variables.

Then equation (17) can be readily integrated between the limits of $l_2=0$ when $t=0$ and $l_2=l_2$ when $t=t$, as follows:

$$\exp\left[-\alpha(P_0-El_2)\right] = \frac{\alpha EK}{2}t\,,$$

which can be expressed in logarithmic form and arranged to give

$$l_2 = \frac{P_0}{E}+\frac{1}{\alpha E}\ln\frac{\alpha EK}{2}+\frac{1}{\alpha E}\ln t\,. \tag{18}$$

Therefore, for a given body under a constant pressure, equation (18) is rewritten as

$$l_2 = A_0+B\log t\,, \tag{19}$$

where $A_0=\dfrac{P_0}{E}+\dfrac{1}{\alpha E}\ln\dfrac{\alpha EK}{2}$ and $B=\dfrac{1}{\alpha E\log e}$.

This equation confirms that there is, under a constant stress, a continuous deformation proceeding in time, though at a decreasing rate. This phenomenon is sometimes described as delayed elasticity in the process of stress application. In this case, if the stress is removed, the strain l_2 will wholly recover in an elastic after effect or creep recovery.

Next, the Maxwell body is suitable for the description of the rheological behavior of the viscous flow, in which the strain rate is proportional to the applied stress. Fig. 18 is the model for the Maxwell body, in which a helical spring and a dash pot are combined in series. When a constant pressure P_0 is added on the body, we obtain

$$P_0 = Ex_1\,, \tag{20}$$

$$\frac{dx_2}{dt} = K \sinh \alpha P_0 , \tag{21}$$

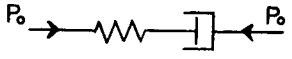

Fig. 18. Model for Maxwell body.

where x_1 is contraction of the spring and x_2 is displacement of the dash pot. Since P_0 is constant, equation (21) gives

$$x_2 = Ct , \tag{22}$$

on integration between the limits of $x_2=0$ when $t=0$ and $x_2=x_2$ when $t=t$, where C is constant.

Thus the resultant displacement of the body is

$$x = x_1+x_2 = \frac{P_0}{E}+Ct , \tag{23}$$

which well represent the steady flow with the internal stress in equilibrium with the applied stress (sometimes spoken of as viscous flow). This deformation, however, is not practically recovered after the removal of the applied stress and, therefore, the permanent deformation will be retained, as described in the previous sections.

Now, a combination of the Kelvin and Maxwell bodies in series may be appropriate for explanation of rheological behaviors in the creep of rocks. This combination is spoken of the Burger's body and it well represents the rheological behavior of concrete as examined by Reiner [1960].

Since the displacement of each of the bodies is additive and each one of them takes the total pressure, the resultant movement of the body in Fig. 19 is given from equations (19) and (23),

$$S = l_2+x = A+B \log t+Ct , \tag{24}$$

where $A=A_0+\frac{P}{E}$.

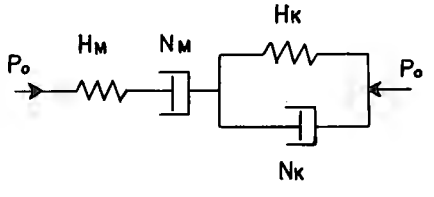

Fig. 19. An elastic flow model assumed to explain the forward process of rock creep.

It is remarkable that the equation (24) of the Burger's body is the same as the

empirical equation of rock deformation. As described in the previous sections, the time-dependent deformations proceed with low speed. Therefore, they can be separated by unloading only and are distinguished as the primary (or the transient) creep which is recoverable after removal of stress and the secondary (or the steady state) creep which remains permanently on unloading. This primary creep can be represented by a Kelvin body, and a Maxwell body will add the effect of the viscous flow, which represents the secondary creep.

On the basis of the rate process theory of viscous flow, it may be inferred that a spring-dash pot combination represents an unit of the material which moves from one equilibrium position to another under an external applied stress and, in which bonds broken in one position are reformed in a successive positions, whereas the pure spring represents a network of bonds which, if broken, do not repair.

Accordingly, the fundamental properties of the rheological models may well account for the effect of fracturing on the deformation of rocks. In other words, the abnormal volume change caused by the fracturing effect in the primary stage of rock creep may be adequately explained by the repairable bonds connected with the pure spring in parallel as shown by N_K and H_K in Fig. 19. On the other hand, the N_M-H_M combination in Fig. 19 is analogous to the fracturing effect with subsequent healing in the secondary stages of rock creep, because the dash pot N_M does not move after removal of total stress and consequently the permanent deformation is retained unless a stress is again applied on the combination in the opposite direction.

5. Sequence structure of the before and after shocks

In Chapter I, a procedure for determining the relative size of elastic strain release increments from earthquake energy was derived and has applied to the series of microearthquakes as well as to the series of severe earthquakes which occurred in a certain region and at the range of a certain depth. And most of the strain release characteristics of the before and after shock sequences for certain time intervals have been shown respectively by

$$S_1 = a+b\log t+ct\,, \tag{25}$$

and

$$S_2 = l+m\log t+ne^{-P\sqrt{T}}\,, \tag{26}$$

where a, b, c, l, m, n and P are appropriate constants of the process and $T=t-t_0$ (t_0 is the interval of the early part of the aftershock sequence).

It is very interesting and important to note that equation (25) is just the same as the strain-time relation of rocks. From this fact, studies of beforeshock sequences

in relation to the creep of rocks are expected to yield valuable information on the tectonic background of the processes and further on the non-elastic behavior of rock bodies of the size of crustal block.

According to Griggs and Handin [1960], the macroscopic deformation of rocks and minerals deformed at high confining pressure can be described in terms of three principal categories of behavior, namely extension fracture, fault and uniform flow. One rock, however, exhibits the entire spectrum of behavior, because its ductility depends upon the magnitudes of the confining pressure and temperature. Therefore, rocks of one kind must be examined under various experimental conditions in order to see the transitional behavior.

Heard [1960] has shown in his experiments by using Solenhofen limestones under various conditions that both temperature and confining pressure greatly affect the brittle-ductile transition of the rock and he has predicted that faulting of dry limestones may take place at a depth of 15 km in the earth's crust and extension fracture may occur at a depth of a few kilometers or less.

On the basis of many experiments, Griggs and Handin [1960] defined the terms as follows:

1) An extension fracture is a separation of a body along a surface parallel to the maximum stress. It occurs under a confining pressure of about a thousand bars or less and at comparatively low temperatures. The strain energy is wholly released concurrently with the occurrence of fractures.

Since the rocks of the earth's crust are under overburden pressure, the macroscopic tensile stresses can exist at depths, perhaps, a few hundred meters especially in the case of the strong crystalline rock. Thus, extremely shallow earthquakes may occur as a result of this mechanism of fracturing.

2) Uniform flow is macroscopically homogeneous deformation. Most rocks tested at 500°C and 5,000 bars or more confining pressure show the deformation of uniform flow and they break down at last without abrupt release of strain energy.

3) When the confining pressure and the temperature are intermediate a fault becomes effective in the mechanism of fracturing of rocks.

A fault is defined as a 'localized offest' parallel to a surface on which the shear stress is maximum and the surface may be inclined at nearly 45° to the direction of maximum compressive stress in homogeneous materials. But this is a special case of faulting in which there may be actual separation because of the total loss of cohesion.

In the process of faulting, the internal friction of rocks plays an important rôle and the angle turns out to be about 30° according to the Coulomb-Mohr criterion, as may be seen in the Appendix of this paper.

Several experiments (Higgs et al., [1958]; Griggs et al., [1960]) have shown direct

evidence that cylinders of various rocks, for example, marble, dolomite and dunite loaded under intermediate confining pressure at temperatures up to 300°C, are broken in compression exhibiting sharp faults which incline at about 30° to the axis of maximum compression and, at the same time, the differential stress drops suddenly to zero with abrupt release of strain energy, but thereafter, the faults reheal and the specimens then continue to support nearly half the original comperssive load. Under an assumption that the confining pressure and the temperature in the earth's crust increase with depths at the rates of 270 atm/km and 25°/km respectively, these conditions at a depth of 10 km can be estimated as 2,700 atms and 250°C.

On the basis of these facts and if the brittle-ductile transition occurs in nature as in these experiments despite the vast difference in strain rate, the faulting can be expected as deep as 10 km in the earth's crust. Accordingly, such a mechanism may well explain the sequence structure of earthquakes of shallow foci.

As was already shown in the previous sections, the deformation of rocks in the process of stress application is certainly caused by the local brittle fractures in rock specimens from the facts that the increments of creep coincide well with the occurrence of elastic shocks and both the cumulative sum of $\sqrt{E}$ of elastic shocks and the creep curve are clearly represented by the same empirical equation of (25). In addition, the strain release characteristics of the beforeshock sequence (or their pattern of $\Sigma\sqrt{E}$) are quite similar to that of the forward process of rock creep as stated above.

Since the faulting is substantially the brittle fracture and it can be expected to occur in the upper part of the earth's crust as described above, it is probably concluded that there is a close analogy in nature between the mechanisms of fracturing of rocks in the laboratory experiments and in the earth's crust, and hence earthquakes of shallow foci are due to fractures with accompanying relief of stress and release of stored energy.

From these points of view, the sequence structure of beforeshocks may be adequately explained by the rheological model shown in Fig.19. In macroscopic view, the dash pots N_K and N_M in Fig. 19, which move from one equilibrium position to another according to the rate process theory, well account for the stepwise increments in the graphs of the cumulative sum of the elastic strain release.

More concretely speaking, in the process of stress application, the spring H_M represents the undelayed elasticity, which is recovered concurrently with the outbreak of the network and produces the main shock, whereas the H_K-N_K combination characterized by the second term of equation (24) represents the delayed elasticity, which is recoverable in an elastic after-effect and probably causes the aftershock sequence as will be shown later. Finally the third term of equation (24) represents

the characteristic of the dash pot N_M and distinguishes clearly the beforeshock sequences from the aftershock sequences. Moreover, the irrecoverable element will produce the permanent deformation on total release of tectonic forces. In fact, there is field evidence for ascertaining the crustal deformation prior to a main shock. Nishimura and Tanaka have made the observations of crustal deformation with tiltmeters at several observatories in Japan. And in their recent article (Nishimura et al., [1963]), they have shown that the anomalous ground tilts were observed prior to the main shock and they might well coincide with the occurrence of beforeshocks. These facts are suggestive for the future study on prediction of destructive earthquakes.

An explanation of aftershock sequences has been suggested by Benioff [1951a, 1951b]. Fig. 20 is the visco-elastic model assumed by him. The G_2-R_2 combination represents the delayed elasticity which is connected to the undelayed elasticity G_1. The body in Fig. 20 is compressed by the tectonic force F resisted by the high viscosity of "secular" dash pot R_1 which does not move substantially within one sequence. The frictional element f represents the seismic fault.

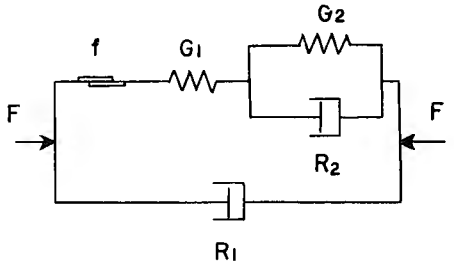

Fig. 20. Visco-elastic model assumed by Benioff to explain aftershock sequences.

After the spring G_1 is discharged concurrently with the outbreak of the main shock, the delayed elasticity is partially discharged and the shear stress required to start sliding of the fault decreases gradually in the course of time. In practice, the intensity of aftershocks never decreases monotonically within a sequence. If the kinematic friction of the element f falls from shock to shock more rapidly than the static friction, stronger shocks can be seen later in spite of the falling force acting on the fault wall.

Benioff has applied this rheological model further to deep and intermediate depth earthquakes. It is no doubt that the material of the earth's mantle shows some delayed elasticity. But at depths of 600～700 km where the pressure is about 200,000 bars and the temperature is estimated as about 500°C or more, all rocks tested, thus far, exhibit the uniform flow and faulting against the dry friction cannot be expected to

occur under these conditions. Whereas, for shallow earthquakes, the models shown in Figs. 19 and 20 may be appropriately applied to the sequence structures of the beforeshocks and aftershocks respectively, though the faulting and secular elements were not specified in Fig. 19.

As already shown in Figs. 9 and 10 or Figs. 12 and 13, the aftershock sequences sometimes have the dual forms which are characterized by the third term of equation (26). Benioff has given an explanation to this phenomenon. The second term of equation (26) corresponds to the compressional strain rebound of the earth's crust, whereas the third term represents the shearing strain recovery which is derived empirically by Michelson [1917] for rocks and other solid materials subjected to torsional stresses. This type of recovery, however, has not been verified by subsequent experiments and therefore the occurrence of dual form in aftershock sequences may remain unexplained.

Nevertheless, it may be inferred that the Bridgman effect concerning an anomalous volume change of rocks stated in the previous sections may provide the basis for a possible mechanical explanation of the interaction between compressive and shearing strains and the delay in onset of so called shearing strain recovery. Just after the main shock, the changes in structure according to the Bridgman's discovery may conspire to lock the shearing strain until the compressional stress decreases to the value where volume changes become normal. Thus, the dual form in case of shallow earthquakes can be adequately explained as the delay in onset of shearing recovery with the help of the Bridgman's discovery, because the effect is sure to play an important rôle, especially in the brittle materials of the earth's crust.

Now, the second terms in both equations (25) and (26), which correspond to the spring-dash pot combinations shown in both models, represent the delayed elasticity of the material of the crust. And if the combination remains unchanged throughout the consecutive sequences (e.g., A_2-A_3 sequences described in Chapter I), the values of b and m in both equations (25) and (26) should be substantially the same. The values of them shown in Figs. 12 and 13 are apparently regarded as good evidence of the validity of this assumption. The determination of these values from the data above mentioned, however, seems not to be reliable because the energy emitted from the hypocenter could not be determined with considerable accuracy.

Chapter III. Summary

The important observational results and their analyses may be summarized as follows:

1) In 1959, about 200 microearthquakes with P-S intervals less than 5 sec. were

recorded at Abuyama Seismological Observatory. They are not aftershocks of a particular severe earthquake and seem to occur nearly stationarily. But, according to the space distribution of their foci and the time series of their occurrence, the microearthquakes are classified into some earthquake sequences which represent the seismic activities of certain regions.

On the other hand, the swarm of severe earthquakes occurred in succession from April to June in 1961 at the region near Himeji, and most of the earthquakes observed at the observatory can be apparently divided into the sequences of two different types.

2) In accordance with the elastic rebound theory, these sequences can be clearly characterized by means of the graphs of cumulative sums of $\sqrt{E}$ for the respective sequences as shown in Figs. 12$\sim$14. From these graphs, it may be inferred that a series of seismic activity is made up of the main shock and its beforeshock and aftershock sequences. Moreover, it must be emphasized that the occurrence patterns of the series of seismic activity in both cases of the microearthquakes and the severe earthquakes are closely resemble each other in their appearances, in spite of the vast difference in released energy summed up for the duration of the respective sequences.

3) According to the laboratory experiments, the deformation of rocks loaded under compression is well represented by equation (10), which is just the same formula as equation (9) of cumulative sum of the released strain for the beforeshock sequence. On the other hand, the deformation of rocks, in the process of stress application, is certainly caused by the local brittle fractures in rock specimens, which are, in turn, ascertained by the observation of elastic shocks as shown in section 3 of chapter II.

Next, the faulting, which is substantially the brittle fractures, can be expected in the upper part of the earth's crust. It is, therefore, concluded that there is a close analogy in nature between the mechanisms of fracturing of rocks in the laboratory experiments and in the earth's crust, and hence earthquakes of shallow foci may be due to fractures, with accompanying relief of stress and release of stored energy.

From these points of view, the sequence structure of beforeshocks may be explained with the rheological model shown in Fig. 19. Among the elements in the model, the dash pot N_M represents the third term of equation (9), which well accounts for the characteristics of the beforeshock sequences as well as that of the creep of rocks in the forward process.

On the other hand, the sequence structure of the aftershocks may be plausibly explained by the model in Fig. 20 according to the Benioff's suggestion. The rheological properties of this model coincide well with the empirical equation (8) for the aftershock sequence.

From the fact that the delayed elasticity of the material of the earth's crust, which

is represented by the spring-dash pot combination in Figs. 19 and 20, plays an important rôle in producing the sequence structure, it may be concluded that a certain series of seismic activity can be clearly characterized by the second terms of both the equations (8) and (9).

4) The facts and their analyses described above may offer suggestions that the routine observation of successive occurrence of earthquakes provides useful data on prediction of destructive earthquakes and many seismic phenomena, especially the sequence structure of the successive occurrence of earthquake swarms, may be adequately explained by the rheological models with the help of the experimental results on rock deformation and an application of the rate process theory to the rheological materials in the earth's interior.

Appendix. A study on the sequence structure of Himeji earthquakes

As shown in the previous chapters, shallow earthquakes are generally caused by the brittle fractures in the earth's crust and the stored energy is emitted in the form of elastic waves, crustal deformations and so on. From this standpoint, the mechanism of earthquake occurrence has been successfully studied by many investigators by means of the patterns of the motions of various phases of seismic waves which are principally determined by the modes of disturbances in the origin. And these problems were summarized by, e.g., Honda in his recent paper [1962].

In fact, the quadrant type pattern of initial P waves has been frequently ascertained for earthquakes of very shallow foci. For explanation of this pattern of initial P waves, there are two prevailing hypotheses on earthquake mechanism.

One of them is a couple of forces with moment acting at the focus, while the other is a set of two couples of forces with moment crossing perpendicularly at the focus,

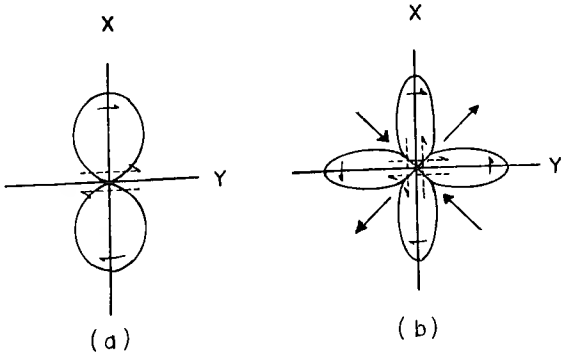

Fig. I. Direction and magnitude of initial S waves: (a) for single couple and (b) for double couple.

and they are called the force systems of type I and type II respectively. Now, the azimuthal distributions of magnitude and direction of initial S waves for both the systems were calculated theoretically by Byerly and Stauder [1958] and are illustrated schematically in Fig. I. In order to ascertain the tectonic forces acting at the focal region, we must, therefore, choose between the force systems of type I and type II by means of the distribution of initial S waves, because both of the force systems equally explain the distribution of initial P waves.

Fig. II is a distribution of initial S waves of the main shock which was accompani-

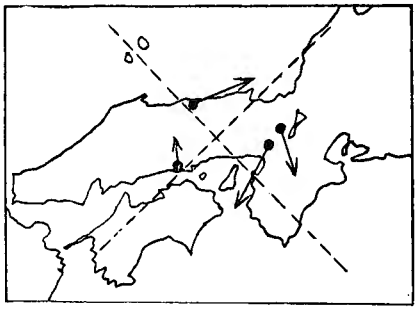

Fig. II. Distribution of initial S waves of the main shock on 7th May 1961.

ed by the earthquake swarms of Himeji sequences and it seems likely that most of the minor shocks show the same distributions of initial S waves as that of the main shock, as was seen in the case of initial P waves. Therefore, it may be inferred that the force system of type I can be assumed to be acting at the focal region for the duration of the sequences.

On the basis of these facts, the distribution of tectonic forces of type I is assumed

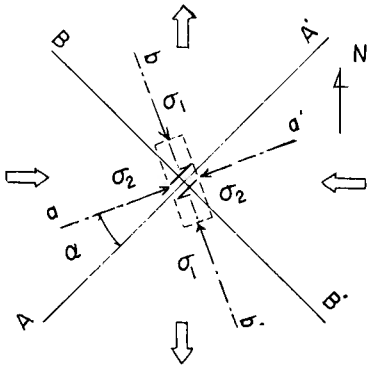

Fig. III. Distribution of tectonic forces assumed to explain the strike slip fault parallel to a nodal line.

to explain the strike slip fault parallel to a nodal line as shown in Fig. III. Hereupon, let us consider a cylinder lying horizontally at the focal region which is studded with epicenters of the main shock and the other minor shocks, and the axis (b-b') coincides with the line of the epicenters as may be seen from Fig. 5. Then, we must take the tectonic forces as $\sigma_2 > \sigma_1 > 0$, because of the fact that the dilatational and compressional areas which are determined by the initial P motions, coincides with the respective quadrants. Accordingly, the tectonic pressure $\sigma_2 - \sigma_1$ may be considered to act on the side of the cylinder, if σ_1 is regarded as the confining pressure at the depth in the earth's crust. Furthermore, this mechanism might be explained equally with the force system acting in extension in the direction of the axis (b-b').

As shown previously, faulting, which is substantially the brittle fracture, can be expected in the uppermost part of the earth's crust and the internal friction (n) of the material plays an important rôle in the process of faulting. In practice, inclination (α) of the fault plane to the direction of the maximum compressional stress is determined by a surface on which the shear stress (τ_α) is maximum, while the normal stress

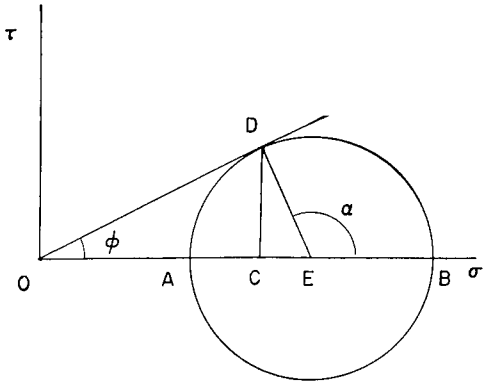

Fig. IV. Mohr's diagram, where $\sigma_\alpha = OC$, $\tau_\alpha = CD$, $\sigma_1 = OA$ and $\sigma_2 = OB$.

(σ_α) becomes minimum. The sliding, therefore, can be expected to start only if the shear stress exceeds the value $n\sigma_\alpha$ according to the theory of dry friction.

Then, the stresses σ_α and τ_α are easily given by use of the applied stresses σ_1 and σ_2,

$$\left.\begin{aligned} \sigma_\alpha &= \frac{\sigma_2+\sigma_1}{2} - \frac{\sigma_2-\sigma_1}{2}\cos 2\alpha\ , \\ \tau_\alpha &= \frac{\sigma_2-\sigma_1}{2}\sin 2\alpha\ . \end{aligned}\right\} \qquad (a)$$

With the help of the Mohr's diagram showing the state of stress as illustrated in Fig. IV, we get

$$n = \tan\phi = \frac{\sigma_2 - \sigma_1}{\sigma_2 + \sigma_1}\frac{1}{\cos\phi},$$

or

$$\sin\phi = \frac{\sigma_2 - \sigma_1}{\sigma_2 + \sigma_1}, \qquad \text{(b)}$$

and

$$\alpha = \pm\frac{\pi}{4} \mp \frac{\phi}{2}. \qquad \text{(c)}$$

As may be clearly seen from Fig. III, the angle α turns out about 25°, and the confining pressure at a depth of 10 km is assumed to be $\sigma_1 = 2{,}700$ bars. By using these values and the relations (b) and (c), the differential stress acting at the cylinder is evaluated as $\sigma_2 - \sigma_1 = 9{,}700$ bars. On the other hand, observations by Griggs et al. [1960] have shown that the strains of the granite and basalt specimens under a confining pressure of 5,000 bars at temperature of 500°C or less, increase linearly with the applied differential stresses up to about 10,000 bars. And they concluded from these facts that the faulting with slight flow might become effective on destruction of these rocks. Moreover, it must be emphasized that the angle α is less than 45° and agrees well with the experimental results on rock specimens as described in section 5 of chapter II (Handin and Hager, [1957]; Higgs and Handin, [1958]). In other words, the strike slip fault parallel to a nodal line (A-A') may be adequately explained by the tectonic forces not in the direction of 45° from the nodal lines, but in the directions of (a-a') and (b-b').

In conclusion, the brief analyses and discussions on the occurrence mechanism of the earthquake swarms will offer valuable suggestions for the future study. But at the same time, several questions are raised: by what cause the internal friction of the materials in the earth's interior acts effectively on the formation of the fault planes, in spite of the fact that the stress rates in the laboratory experiments and in the field differ vastly from each other. Is there any relation between the shallow earthquake and the deep one with respect to the angle α? Is the assumption of the force system of type I valid even for the other sequences? For explanation of these problems, we need more detailed data as well as a theoretical basis for the internal friction.

Acknowledgements

The present writer would like to express his cordial thanks to Dr. Kenzo Sassa, the Emeritus Professor of Kyoto University, for his generous advice. The writer's thanks are also due to Professor Haruo Miki and Dr. Kennosuke Okano of Kyoto University for their encouragements throughout the present study. He is much indebted to the director of Osaka Branch of Japan Meteorological Agency for permission for copying the seismograms.

References

Asada, T., 1957; Observation of near-by microearthquakes with ultra sensitive seismometers, Jour. Phys. Earth, 5, 83.

Asada, T. et al., 1954; Observations of near-by microearthquakes occurring in the Vicinity of Matsushiro, Japan, Jour. Seis. Soc. Japan, Ser. 2, 11, 7. (in Japanese)

Benioff, H., 1951a; Crustal strain characteristics derived from earthquake sequence, T.A.G.U., 32, 508.

Benioff, H., 1951b; Earthquake and rock creep, B.S.S.A., 41, 31.

Bridgman, P. W., 1949; Volume changes in the plastic stages of simple compression, Jour. Appl. Phys., 20, 1241.

Byerly, P. and W. Stauder, 1958; The mechanism at the focus of an earthquake, Earthquake Notes (Eastern Section, Seismol. Soc. Am.), 29, 17.

Grasstone, S., K. J. Laidler and H. Eyring, 1941; Theory of rate processes, McGraw-Hill, New York.

Griggs, D., 1940; Experimental flow of rocks under conditions favouring recrystallization, B.G. S.A., 51, 1002.

Griggs, D. et al., 1960; Deformation of rocks at 500°C to 800°C, The Geological Society of America, Memoir, 79, 39.

Griggs, D. and J. Handin, 1960; Observations on fracture and a hypothesis of earthquakes, The Geological Society of America, Memoir, 79, 347.

Handin, J., 1957; Experimental deformation of rocks and minerals, Colo. School Mines, Quart., 5, 75.

Handin, J. and R. V. Hager, 1957; Experimental deformation of rocks under confining pressure, Bull. Assoc. Petroleum Geologist., 41, 1.

Heard, H. C., 1960; Transition from brittle fracture to ductile flow in Solenhofen limestone as a function of temperature. Confining pressure and interstitial fluid pressure, The Geological Society of America, Memoir, 79, 193.

Higgs, D. V. and J. Handin, 1958; Experimental deformation of dolomite single crystals, B.G.S.A., 70, 245.

Honda, H., 1962; Earthquake mechanism and seismic waves, Jour. Phys. Earth., 10, No. 2.

Ishimoto, M. and K. Iida, 1939; Observations sur les seismes energistré par le microseismograph construit dernièrement (1), B.E.R.I., 17, 443.

Kanai, K. et al., 1954; Measurement of the micro-tremor I, B.E.R.I., 32, 199.

Kawasumi, H., 1952; Energy law of earthquake occurrence in the Vicinity of Tokyo, B.E.R.I., 30, 325.

Komura, S., 1954; Some stochastic results of the maximum amplitude index in the Ishimoto-Iida's statistical formula (1), Jour. Seis. Soc. Japan, Ser. 2, 7, 194. (in Japanese)

Komura, S., 1955; ibid., (2), Jour. Seis. Soc. Japan, Ser. 2, 8, 55. (in Japanese)

Lomnitz, C., 1956; Creep measurements in igneous rocks, Jour. Geol., 64, 473.

Matsushima, S., 1960; On the flow and fracture of igneous rocks, Bulletin of the Disaster Prevention Research Institute, Kyoto Univ., 36, 1.

Michelson, A. A., 1917; Elastic viscous flow, Part I, Jour. Geol., 405.

Miyamura, S., 1962; Seismicity and geotectonics, Jour. Seis. Soc. Japan, Ser. 2, 15, 32. (in Japanese)

Mogi, K., 1962a; Study of elastic shocks caused by the fracture of heterogeneous materials and its relation to earthquake phenomena, B.E.R.I., 40, 125.

Mogi, K., 1962b; The fracture of a semi-infinite body caused by an inner stress origin and its relation to the earthquake phenomena, B.E.R.I., 40, 816.

Nishimura, E. and Y. Tanaka, 1963; On peculiar mode of secular ground tilting connected with a sequence of earthquakes in some restricted areas, Special Contributions of the Geophysical Institute, Kyoto Univ., 2, 172.

Omote, S. et al., 1956; Earthquake observations in Kawasaki and Turumi areas and the seismic qualities of the ground, B.E.R.I., 34, 335.

Orowan, E., 1949; Fracture and strength of solid, The Phys. Soc. Repts. on Progress in Physics, V, 12, 185.

Reid, H. F., 1911; The elastic-rebound theory of earthquake, Univ. Calif. Pub. Dept. Geol. Sci., 6, 512.

Reiner, M., 1960; The rheology of concrete, 'Rheology Vol. III', Academic Press, New York, 341.

Robertson, E. C., 1960; Creep of Solenhofen limestone under moderate hydrostatic pressure, The Geological Society of America, Memoir, 79, 227.

Tsuboi, C., 1956; Earthquake energy, earthquake volume, aftershock area and strength of the earth's crust, Jour. Phys. Earth, 4, 63.

Watanabe, H., 1963; The occurrence of elastic shocks during destruction of rocks and its relation to the sequence of earthquakes, Special Contributions of the Geophysical Institute, Kyoto Univ., 3, 297.